

Revista Mexicana de Astronomía y Astrofísica

Revista Mexicana de Astronomía y Astrofísica
Universidad Nacional Autónoma de México
rmaa@astroscu.unam.mx
ISSN (Versión impresa): 0185-1101
MÉXICO

2002

A. Riera / P. García Lario / A. Manchado / M. Bobrowsky / R. Estalella
NEW OBSERVATIONS OF THE HIGH-VELOCITY OUTFLOWS OF THE PROTO-
PLANETARY NEBULA HEN 3-1475

Revista Mexicana de Astronomía y Astrofísica, volumen 013
Universidad Nacional Autónoma de México
Distrito Federal, México
pp. 127-132

Red de Revistas Científicas de América Latina y el Caribe, España y Portugal

Universidad Autónoma del Estado de México

reDalyC
LA HEREDERA CIENTÍFICA DE UNAM
<http://redalyc.uaemex.mx>

NEW OBSERVATIONS OF THE HIGH-VELOCITY OUTFLOWS OF THE PROTO-PLANETARY NEBULA HEN 3-1475

A. Riera,^{1,2} P. García-Lario,³ A. Manchado,⁴ M. Bobrowsky,⁵ and R. Estalella²

RESUMEN

La nebulosa proto-planetaria Hen 3-1475 presenta un jet óptico con un alto grado de colimación formado por una serie de condensaciones excitadas por ondas de choque. Las zonas internas del jet muestran altísimas velocidades radiales. En este trabajo presentamos el análisis detallado de la estructura cinemática y de las condiciones de excitación de las condensaciones en base a datos espectroscópicos de alta resolución espectral y a las imágenes de alta resolución espacial obtenidas con el *HST*. Discutimos las semejanzas entre el jet de Hen 3-1475 y los jets HH. Ambos presentan perfiles extremadamente anchos con dos picos en emisión, una disminución de las velocidades radiales con la distancia a la fuente central de forma escalonada, y en ambos se hallan velocidades tangenciales altas. La interpretación conjunta de estas propiedades apunta a la variabilidad temporal de la velocidad de eyección como mecanismo responsable de la formación de este jet.

ABSTRACT

The proto-planetary nebula Hen 3-1475 shows a remarkable highly collimated optical jet with a S-shaped string of shock-excited knots. Moreover, extremely high velocities have been observed in the innermost regions of its jet. We present a detailed analysis of the kinematic structure, and the excitation conditions in the shock-excited knots based on ground-based high dispersion spectroscopy and high angular resolution images obtained with the *HST* WFPC2. We discuss the similarities between the jet of Hen 3-1475 and the HH jets. Both exhibit double-peaked and extremely wide profiles, a decrease of the radial velocities with distance to the source in a step-like fashion, and high tangential velocities. The overall picture of Hen 3-1475 supports the description of the system as the result of time-dependent ejection velocity variability.

Key Words: ISM: JETS AND OUTFLOWS — PLANETARY NEBULAE: INDIVIDUAL (HEN 3-1475) — SHOCK WAVES

1. INTRODUCTION

Hen 3-1475 is a highly collimated bipolar PPN, which displays a spectacular S-shaped string of point-symmetric knots extending over $17''$, observed from the ground by Bobrowsky et al. (1995) and Riera et al. (1995). With the help of *HST* WFPC2 observations it is now possible to resolve the sub-arcsecond structure of the outer knots and the inner regions (Borkowski et al. 1997). The most spectacular features observed in Hen 3-1475 are its very high velocity outflows (Riera et al. 1995; Bobrowsky et al. 1995; Riera et al. 2000; Borkowski & Harrington 2001).

The strong far infrared excess detected by *IRAS* is interpreted as the remnant emission from the AGB circumstellar shell, while the known presence of strong P-Cygni profiles in the Balmer lines indicates

that mass loss is still on-going. This is confirmed by the detection of thermal emission from hot dust in the near infrared. The molecular gas in the envelope has been detected in CO as an expanding torus of material. In addition, Hen 3-1475 also exhibits strong OH maser emission (te Lintel Hekkert 1991; Bobrowsky et al. 1995). Both CO and OH show a broad (60 km s^{-1}) component indicative of a fast molecular outflow, which appears to be extended. VLA observations revealed the presence of a compact source close to the central star (Bobrowsky et al. 1995; Knapp et al. 1995), indicating that the central star became hot enough to ionize the gas in its vicinity. These observations, together with the indications of nitrogen overabundance, indicate that the central star is undergoing the transition from the AGB phase to the PN stage.

2. FLOW GEOMETRY AND KINEMATICS

The F658N *HST* image shows clearly the jet-like structure and three pairs of symmetric emission knots (see Figure 1). The detailed study of the innermost regions reveals the presence of converging lines

¹Universitat Politècnica de Catalunya, Spain.

²Universitat de Barcelona, Spain.

³ISO Data Centre, ESA, Spain.

⁴Instituto de Astrofísica de Canarias, Spain.

⁵Challenger Center for Space Science Education, USA.

connecting the innermost knots and the core region in the NW and SE lobes (Borkowski et al. 1997). The nomenclature used for the knots maintains the single number names used by Borkowski et al. (1997). The SE1 knot shows subarcsecond structure, with the existence of three compact condensations which are labelled with a letter after the number.

2.1. Proper Motion Measurements

We have derived the proper motions of the knots of the Hen 3-1475 jet based on F658N ($\lambda_c = 6590 \text{ \AA}$, $\delta\lambda = 28.5 \text{ \AA}$) images obtained on 1996 June 6 and 1999 September 19 with the *HST* using the WFPC2. The F658N images were retrieved from the *HST* Data archive. Their spatial resolution is $0''.045 \text{ pixel}^{-1}$. In order to carry out the proper motion measurements, the first- and second-epoch F658N *HST* images were converted into a common reference system, with the Hen 3-1475 jet along the y axis, oriented at a P.A. of 136° . After the transformation, the average and rms of the difference in position for the reference stars in the two images was -0.318 ± 0.08 pixels in the x coordinate and 0.096 ± 0.06 pixels in the y coordinate.

We defined boxes which included the emission of the individual condensations in each epoch, we computed the two-dimensional cross-correlation function of the emission within the boxes, and finally we determined the proper motion through a parabolic fit to the peak of the cross-correlation function. The uncertainty in the position of the correlation peak has been estimated through the scatter of the correlation peak positions obtained from boxes differing from the nominal one in 0 or ± 2 pixels ($0''.090$) in any of its four sides. The error adopted has been twice the rms deviation of position, for each coordinate, added quadratically to the rms alignment error.

The results obtained for the knots along the Hen 3-1475 jet are shown in Table 1. Our proper motion measurements for NW2 and SE2 are compatible with the results obtained by Borkowski & Harrington (2001). The tangential velocity has been calculated assuming a distance to Hen 3-1475 of 5 kpc (Riera et al. 1995; Riera et al. in preparation). However, the distance to Hen 3-1475 is not well determined. A distance to Hen 3-1475 of ~ 8 kpc has been deduced by Borkowski & Harrington (2001) from the combination of their proper motion measurements and the ground-based spectroscopy (adopting an inclination of the jet axis to the plane of sky of 50°). In Fig. 1 we show the F658N *HST* 1999 image of Hen 3-1475, with each knot identified with a label. The arrows indicate the proper motion velocity of each knot, and

Hen 3-1475 (1999)

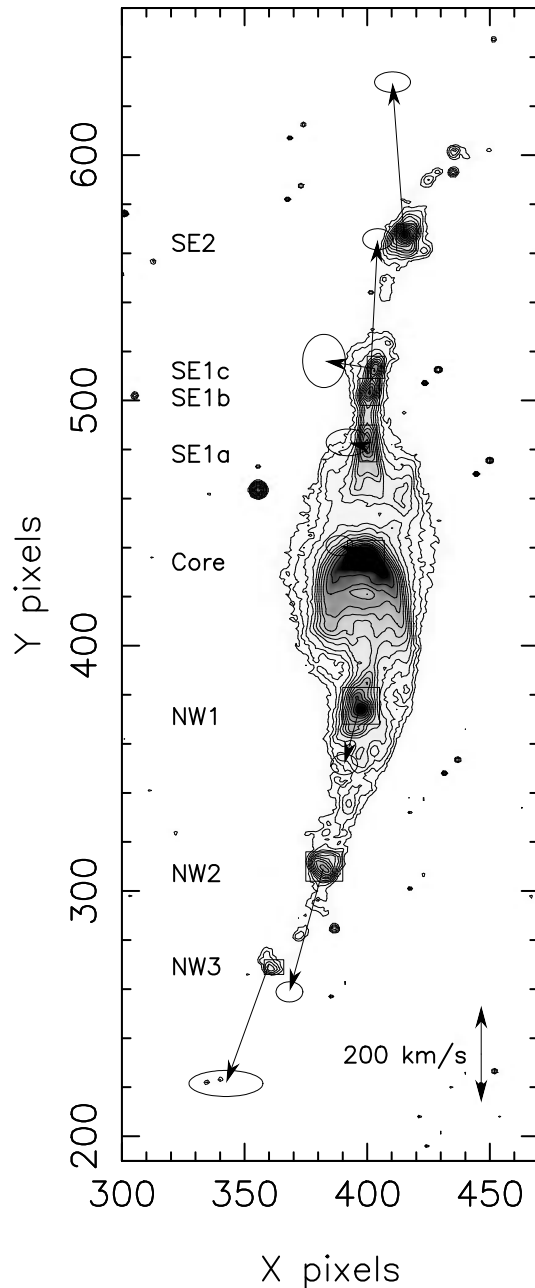


Fig. 1. F658N *HST* WFPC2 image from 1999 observations (P.I. Harrington). The contour spacing is logarithmic. The arrows indicate the proper motion velocity of each knot. The ellipses at the end of each arrow indicate the uncertainty in the components of the velocity vector. Both axes are labelled in pixels. The spatial resolution is $0''.045 \text{ pixel}^{-1}$.

TABLE 1
PROPER MOTION MEASUREMENTS OF
HEN 3-1475

Knot	μ_x^a	μ_y^a	V_{\tan}^b	P.A. ($^\circ$)
SE2	-1.0 ± 2.6	13.2 ± 0.9	315 ± 60	132 ± 9
SE1C	-4.3 ± 2.8	0.6 ± 4.2	104 ± 143	33 ± 35
SE1B	0.7 ± 1.0	13.2 ± 0.6	314 ± 44	139 ± 7
SE1A	0.7 ± 2.8	0.4 ± 4.8	40 ± 84	60 ± 20
NW1	-1.3 ± 1.2	-4.9 ± 0.8	121 ± 34	-28 ± 16
NW2	-2.9 ± 1.1	-10.6 ± 0.9	260 ± 34	-28 ± 5
NW3	-3.7 ± 1.1	-10.2 ± 0.9	258 ± 41	-24 ± 8

^amas yr⁻¹. ^bkm s⁻¹.

the ellipses at the end of each arrow indicate the uncertainty in the components of the velocity vector.

The overall movement of the knots is close to the axis of the jet with a small westward tilt. The innermost knots SE1a and SE1c do not show significant proper motions, while the inner knot SE1b and the intermediate knot SE2 show tangential velocities of ~ 315 km s⁻¹. The intermediate knot NW2 and the outermost knot NW3 show proper motions of ~ 260 km s⁻¹, while the innermost knot NW1 show a smaller but significant tangential velocity.

2.2. Radial velocities

We obtained long-slit spectra along the bipolar axis with the Intermediate Dispersion Spectrograph at the 2.5 m Isaac Newton Telescope (Observatorio del Roque de los Muchachos, La Palma), with an effective spectral resolution of 20 km s⁻¹, covering the [N II] 6548, 6583 Å, H α , [S II] 6717, 6731 Å, and [O I] 6300 Å emission lines. The spatial resolution was 0'':33 pixel⁻¹ (see Riera et al. (2000) for the description of the observations). The radial velocities of the gas as a function of position have been obtained following the standard method of extracting the kinematical information by fitting multiple gaussians to the observed emission line profiles. Figure 2 shows the radial velocity as a function of distance to the central source for the [N II] 6583 Å, [S II] 6717 Å, and [O I] 6300 Å emission lines. Radial velocities are quoted with respect to the systemic radial velocity (= 44 km s⁻¹). The 1-D trace from the F658N *HST* image is plotted to aid in the identification of the emission knots admitted by the slit. The position-velocity diagrams of [N II] 6583 Å, [S II] 6717 Å, and [O I] 6300 Å differ rather little. The basic features—discussed below—appear in all emission lines we have studied, including H α (described in Riera et al. 2000).

Middle knots and outermost regions: The middle knots exhibit double-peaked profiles. The two components are centered at mean relative radial velocities of 550 and 365 km s⁻¹. Moreover, the difference between the low and high velocity peaks, decreases with increasing distance to the source. A detailed inspection of Fig. 2 show that the velocity of the low component seems to linearly increase with increasing distance to the center, while the velocity of the high-velocity component (redward in SE2 and blueward in NW2) remains almost constant. The emission lines from the intermediate knots show very wide profiles. The total range in velocity exhibited by the intermediate knots expands from 190 to 665 km s⁻¹.

At the outermost regions the two components merge with one another. At distances of $\pm 9''$ from the center, the emission lines show one-peaked broad profiles at radial velocities ± 405 km s⁻¹ relative to the systemic radial velocity, with a velocity dispersion of ~ 450 km s⁻¹.

Innermost regions: The innermost knots are characterized by very high radial velocities and extremely wide emission line profiles. In the innermost regions (from 1 to 4'') the low velocity emission vanishes near $\sim -44(+29)$ km s⁻¹ and the high velocity gas can be traced up to $-951(+1009)$ km s⁻¹ for NW1 (SE1a). The strongest emission occurs in the high velocity component, which is centered at -942 km s⁻¹ in NW1 and $+926$ km s⁻¹ in SE1a. There is a hint of a double-peaked profile, whose peaks are wider and more widely separated in velocity than those of the intermediate knots. The high- and low-velocity components are marked with an arrow in Fig. 2. The low-velocity peaks are centered at $\simeq -200$ km s⁻¹ and 450 km s⁻¹ in NW1 and SE1a respectively.

Fig. 2 also illustrates the behavior of the strong high-velocity component with distance from the central source. There is a remarkable decrease of the radial velocities with distance to the source for distances from 1'' to 4''. The highest radial velocity of the innermost condensations of the southern lobe is found at the position of SE1a (with a relative radial velocity of $+926$ km s⁻¹). Downstream (along condensations SE1b and SE1c) the radial velocity smoothly decreases with distance to the source (from $+926$ km s⁻¹ to $+780$ km s⁻¹ in only 1''). A similar but symmetric behaviour is observed in NW1, which shows a radial velocity of -942 km s⁻¹ in the innermost region and decreases to -817 km s⁻¹ in 3''.

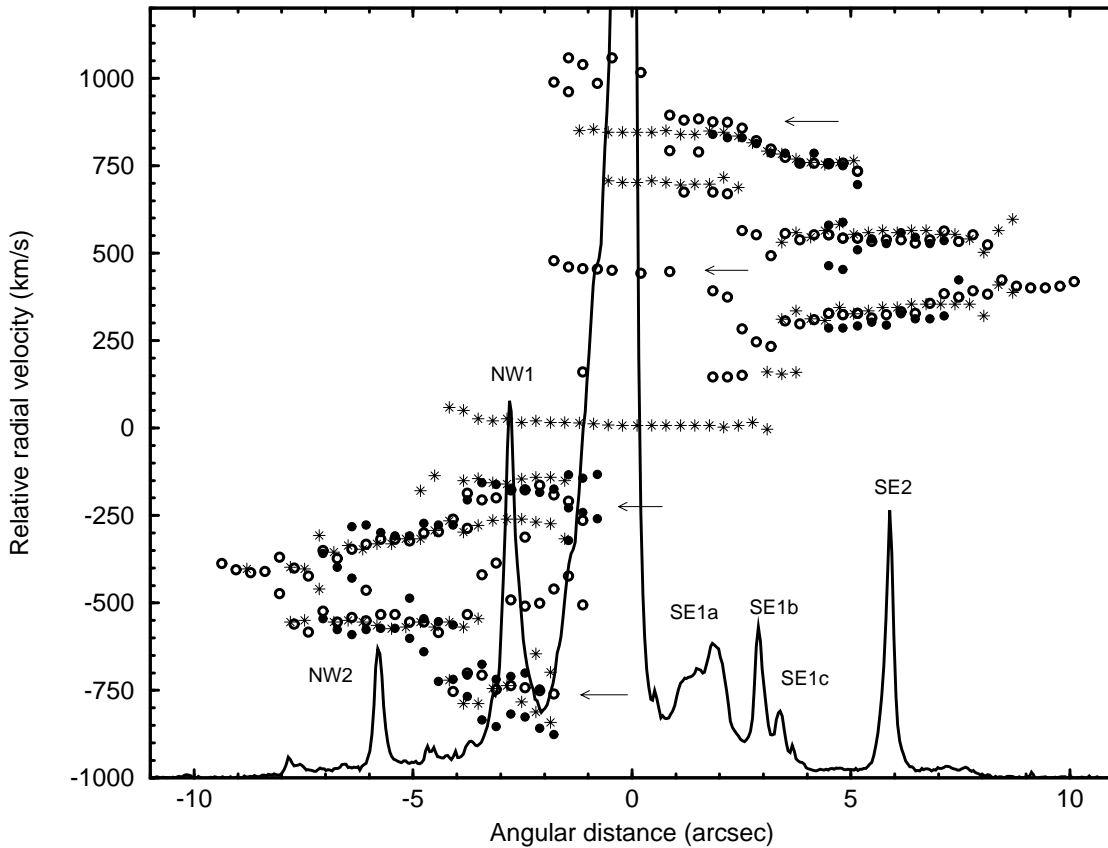


Fig. 2. Relative radial velocities versus distance from the source position along the axis of the nebula. Relative velocities and position are quoted with respect to the systemic radial velocity ($= 44 \text{ km s}^{-1}$) and to the position of the central star, respectively. Open circles: [N II] 6583 Å, filled circles: [S II] 6717 Å, and stars: [O I] 6300 Å.

3. SHOCK VELOCITIES

The emission observed from the jet of Hen 3-1475 is formed in the recombination region of shock waves (Riera et al. 1995). The observed spectra are characterized by extremely large [N II] 6583 Å/ $H\alpha$ ratios (~ 3.0), and electron densities of $\sim 3000 \text{ cm}^{-3}$.

We have obtained a grid of (steady 1D) plane-parallel shock models with the photoionization-shock code MAPPINGS 1c (Binette, Dopita, & Tuohy 1985; Dopita, Binette, & Tuohy 1984). We have adopted a preshock density of 50 cm^{-3} and the mean Type I PNe abundances (Kingsburgh & Barlow 1994). By comparing the observed emission line ratios for the intermediate knots (Table 4 from Riera et al. 1995) with the predictions of planar shock models, we attempt to determine the velocity of the shocks responsible for the observed spectra.

The results are shown in Figure 3, where the observed and predicted emission line ratios are plotted for comparison. Fig. 3 illustrates that the observed [N II] 6583 Å/ $H\alpha$ ratios are roughly repro-

duced for a wide range of shock velocities (from 100 to 250 km s^{-1}), while the values of the temperature-dependent ratio $[\text{N II}](6584 + 6548)/5755$ are only marginally reproduced for a shock velocity $\sim 100 \text{ km s}^{-1}$. The [N I] 5200 Å/ $H\alpha$ ratios are reproduced for shock velocities from 100 to 150 km s^{-1} . These results confirm that the gas is nitrogen enriched.

Furthermore, the observed [O III] 5007 Å/ $H\alpha$ ratios are reproduced for shock velocities higher than 120 km s^{-1} . The models predict too low [O I] 6300 Å/ $H\alpha$ and [S II] (6717 + 6731)/ $H\alpha$ emission line ratios. The weakness of the [O I] and [S II] predicted for shock models, with a severe disparity between the observed and predicted emission line intensities, is not surprising since shock models appear to have problems in reproducing the observed line ratios in SN remnants and HH objects (see, e.g., Dopita et al. 1984; Raga, Böhm, & Cantó 1996).

The attempt to model the observed emission line ratios using plane parallel shocks has been partially successful. The spectra might arise in the recombi-

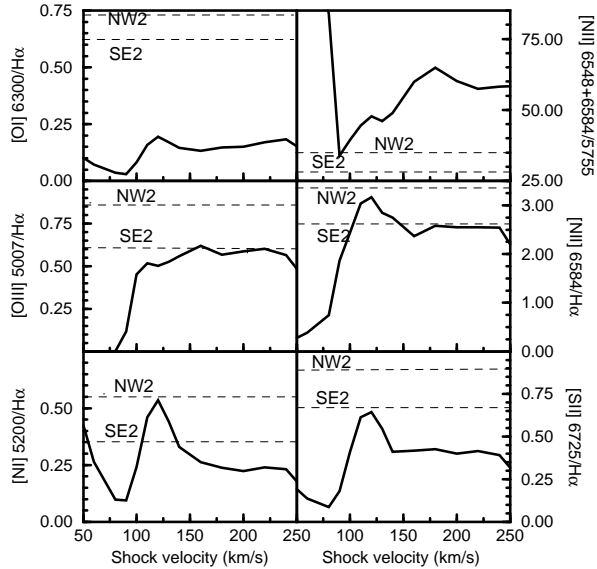


Fig. 3. Predicted emission line ratios for a grid of 1-D steady shock models as a function of shock velocity (solid line). Dashed lines are the observed emission line ratios for NW2 and SE2.

nation region of a shock wave with velocity ranging from 100 to 150 km s^{-1} , moving through a nitrogen enriched gas.

4. DISCUSSION

The main results we have obtained from long-slit spectroscopy and the proper motion measurements are summarized below:

(i) The profiles are double-peaked with extremely wide emission line profiles in both the innermost and intermediate condensations. In the middle knots emission lines extend from 665 to 190 km s^{-1} , and in the innermost regions (at distances of $\sim 3''$ from the central source) a velocity dispersion of $\sim 900 \text{ km s}^{-1}$ is observed.

(ii) Within the intermediate condensations there is a systematic, slow variation of the velocity of the low-velocity component.

(iii) The radial velocity of different knots decreases with increasing distance from the source in a step-like fashion, showing an abrupt velocity variation (of $\sim 350 \text{ km s}^{-1}$) at the position of the intermediate knots. The radial velocity decreases by 146 km s^{-1} and 125 km s^{-1} along SE1 and NW1, respectively.

(iv) High proper motions have been measured for several condensations (see Table 1). Tangential velocities of $\sim 260 \text{ km s}^{-1}$ have been measured in NW2 and NW3 and $\sim 315 \text{ km s}^{-1}$ in SE1b and SE2. No

variation of the tangential velocity with distance to the source has been detected.

(v) The emission line spectra are (qualitatively) reproduced by plane parallel shock waves.

Some of the properties enumerated above have been observed in HH objects. HH objects show prominent double-peaked profiles, where the high velocity and low velocity components are spatially displaced (see, e.g., Solf et al. 1986; Heathcote et al. 1998). Some HH objects show extraordinarily large velocity dispersion (e.g., HH 80-A and HH 81-A reach a velocity dispersion of 700 km s^{-1}), and a slow but systematic decrease of the radial velocity along the condensation (e.g., in HH 32: Solf et al. 1986). High radial velocities and the presence of abrupt variations at the position of the internal knots of the jet have been observed in several HH jets (e.g., HH 46/47, HH 32, HH 34: Heathcote & Reipurth 1991; 1992; Solf et al. 1986; Hartigan et al. 1986), and several of these knots of the HH jets show high proper motions (see, e.g., Eislöfel et al. 1994; López et al. these proceedings). The relevant similarities between HH jets and the jet of Hen 3-1475 point towards a common mechanism responsible for the formation of the knots. Different scenarios have been proposed to explain the formation of string of aligned knots in HH jets (see, e.g., Raga 1995). The proper motions, the variation of the radial velocity with increasing distance from the source and the abrupt velocity variation favours the intrinsic velocity variability (Raga 1993). In the time-dependent analytical approaches and numerical simulations the knots are internal working surfaces that result from a time dependent source. The predictions from the time dependent models are in qualitative agreement with the observations (Raga 1993).

We therefore propose that the emission knots observed in Hen 3-1475 arise from internal working surfaces (at least for the knots showing significant proper motions) in a time dependent flow. It is possible that some of the radial velocity variations detected along the jet of Hen 3-1475 are due to energy losses along the flow and precession, but the abrupt decrease is the most compelling evidence for velocity variability. The overall picture supports the description of the system as the result of time-dependent ejection velocity and direction.

AR and RE are partially supported by DGI-CYT grant PB98-0670. MB is supported by STScI grant number GO-06364.03-A. This work was partially funded through grant PB97-1435-C02-02 from the Spanish Dirección General de Enseñanza Supe-

rior (DGES). This work is based on observations made during service time with the 2.5-m Isaac Newton Telescope operated on La Palma by the Isaac Newton Group of Telescopes in the Observatorio del Roque de los Muchachos of the Instituto de Astrofísica de Canarias, Spain, and observations made with the *Hubble Space Telescope*, obtained from the Data Archive at the Space Telescope Science Institute, which is operated by the Association of Universities for Research in Astronomy, Inc., under NASA contract NAS5-26555.

REFERENCES

- Binette, L., Dopita, M. A., & Tuohy, I. R. 1985, *ApJ*, 297, 476
- Bobrowsky, M., et al. 1995, *ApJ*, 446, L89
- Borkowski, K. J., Blondin, J. M., & Harrington, J. P. 1997, *ApJ*, 482, L97
- Borkowski, K. J. & Harrington, J. P. 2001, *ApJ*, 550, 778
- Dopita, M. A., Binette, L., & Tuohy, I. R. 1984, *ApJ*, 282, 142
- Eislöfel, J., Mundt, R., & Böhm, K.-H. 1994, *AJ*, 108, 1042
- Hartigan, P., Mundt, R., & Stocke, J. 1986, *AJ*, 91, 1357
- Heathcote, S., & Reipurth, B. 1991, *A&A*, 246, 511
- _____. 1992, *AJ*, 104, 2193
- Heathcote, S., Reipurth, B., & Raga, A. C. 1998, *AJ*, 116, 1940
- Kingsburgh, R. L., & Barlow, M. J. 1994, *MNRAS*, 271, 257
- Knapp, G. R., Bowers, P. F., Young, K., & Phillips, T. G. 1995, *ApJ*, 455, 293
- López, J. A. et al. 2002, *RevMexAA(SC)*, 13, 139 (this volume)
- Raga, A. C. 1993, *Ap&SS*, 208, 163
- _____. 1995, *RevMexAA(SC)*, 1, 103
- Raga, A. C., Böhm, K.-H., & Cantó, J. 1996, *RevMexAA*, 32, 161
- Riera, A., García-Lario, P., Manchado, A., Pottasch, S. R., & Raga, A. C. 1995, *A&A*, 302, 137
- Riera, A., García-Lario, P., Manchado, A., & Bobrowsky, M. 2000, in *Astrophysics and Space Science Library* Vol. 265, *Post-AGB objects (Proto-Planetary Nebulae) as a Phase of Stellar Evolution*, eds. R. Szczerba & S. K. Górný (Dordrecht: Kluwer), 209
- Solf, J., Böhm, K.-H., & Raga, A. C. 1986, *ApJ*, 305, 795
- Te Lintel Hekkert, P. 1991, *A&A*, 248, 209

- A. Riera: Departament de Física i Enginyeria Nuclear. Universitat Politècnica de Catalunya, Escola Universitària Politècnica de Vilanova i La Geltrú, Av. Víctor Balaguer s/n, E-08800 Vilanova i la Geltrú, Spain (angels.riera@upc.es).
- P. García-Lario: ISO Data Centre, Astrophysics Division, Space Science Department of ESA, Villafranca del Castillo, Ap. de Correos 50727, E-28080 Madrid, Spain.
- A. Manchado: Instituto de Astrofísica de Canarias, E-38200 La Laguna, Spain.
- M. Bobrowsky: Challenger Center for Space Science Education, 1250 North Pitt Street, Alexandria, VA 22314, USA.
- R. Estalella: Departament d'Astronomia i Meteorologia, Universitat de Barcelona, Av. Diagonal 647, E-08028 Barcelona, Spain.